

Neutron emissions in brittle rocks during compression tests: Monotonic vs cyclic loading

*Original*

Neutron emissions in brittle rocks during compression tests: Monotonic vs cyclic loading / Carpinteri, Alberto; Borla, Oscar; Lacidogna, Giuseppe; MANUELLO BERTETTO, AMEDEO DOMENICO BERNARDO. - In: PHYSICAL MESOMECHANICS. - ISSN 1029-9599. - STAMPA. - 13:(2010), pp. 268-274. [10.1016/j.physme.2010.11.007]

*Availability:*

This version is available at: 11583/2440639 since:

*Publisher:*

Elsevier

*Published*

DOI:10.1016/j.physme.2010.11.007

*Terms of use:*

This article is made available under terms and conditions as specified in the corresponding bibliographic description in the repository

*Publisher copyright*

(Article begins on next page)

# Neutron emissions in brittle rocks during compression tests: Monotonic vs. cyclic loading

A. Carpinteri<sup>1\*</sup>, O. Borla<sup>1,2</sup>, G. Lacidogna<sup>1</sup> and A. Manuello<sup>1</sup>

<sup>1</sup> Politecnico di Torino, Torino, 10129, Italy

<sup>2</sup> Istituto Nazionale di Fisica Nucleare, Torino, 10125, Italy

Neutron emission measurements, by means of  $^3\text{He}$  devices and bubble detectors, were performed during two different kinds of compression tests on brittle rocks: under monotonic and cyclic loading. The material used for the tests was Green Luserna Granite, with different specimen sizes and shapes, and consequently with different brittleness numbers. Since the analyzed material contains iron, our conjecture is that piezonuclear reactions involving fission of iron into aluminum, or into magnesium and silicon, should have occurred during compression damage and failure. Some studies have been already conducted on the different forms of energy emitted during the failure of brittle materials. They are based on the signals captured by acoustic emission measurement systems, or on the detection of electromagnetic charge. On the other hand, piezonuclear neutron emissions from very brittle rock specimens in compression have been discovered only very recently. In this paper, the authors analyse this phenomenon from an experimental point of view.

*Keywords:* neutron emission, piezonuclear reactions, rocks crushing failure, strain localization

## 1. Introduction

This paper discusses the phenomenon of neutron emissions from brittle rock specimens under mechanical loading from an experimental point of view. The aim is to emphasize the neutron emissions from piezonuclear reactions, that have been recently observed for the first time and published in [1–4], providing new experimental evidences.

The different forms of energy emitted during the failure of brittle materials have been mainly measured based on the signals captured by the acoustic emission measurement systems [5–14], or on the detection of the electromagnetic charge [15–22]. The acoustic emission technique analyses the transient elastic waves due to stress redistribution following fracture propagation. Many experiments in measuring the released energy from fracture of brittle rocks conducted by acoustic emission have had a pioneering role [5–7]. Nowadays, the acoustic emission technique is well-known in the scientific community and applied for monitoring purpose also in concrete structures [8]. In addition,

considering applications of damage mechanics to material failure, and exploiting the analogy between acoustic emission and seismicity, acoustic emission associated with microcracks is monitored and power-law frequency magnitude statistics are observed [9–14]. The electromagnetic signals are related to brittle materials in which the fracture propagation occurs suddenly and it is accompanied by abrupt stress drops in the stress-strain curve. A number of laboratory studies revealed the existence of electromagnetic signals during fracture experiments carried out on a wide range of materials [15]. Moreover, it was observed that the electromagnetic signals detected during failure of materials are analogous to the anomalous radiation of geoelectromagnetic waves observed before major earthquakes [16], reinforcing the idea that the electromagnetic effect can be applied as a forecasting tool for earthquakes. A relevant attempt to explain the electromagnetic signals origin is assumed to be caused by net charges of opposite sign appearing on the vibrating faces of opening fractures [17–20]. According to this model, the electromagnetic signals amplitude increases as long as fracture propagates, since the rupture of new atomic bonds contributes to the electromagnetic emissions. When the fracture arrests, the acoustic emission waves and the electromagnetic signals decay by relaxation [21, 22].

---

\* Corresponding author

Prof. Alberto Carpinteri, e-mail: alberto.carpinteri@polito.it

As regards the neutron emissions, we present new experiments, performed by means of  $^3\text{He}$  neutron detectors and bubble type BD thermodynamic neutron detectors, on brittle rock test specimens. Two different kinds of mechanical tests were carried out: compression tests under monotonic and under cyclic loading. The material used for the compression tests was a non-radioactive Green Luserna Granite, with different specimen sizes and shapes, and consequently with different brittleness numbers. The compression tests were performed at the Fracture Mechanics Laboratory of the Politecnico di Torino [4].

For specimens of larger dimensions, neutron emissions, detected by  $^3\text{He}$ , were found to be of about one order of magnitude higher than the ordinary natural background level at the time of the catastrophic failure. As regards test specimens with more ductile behaviour, neutron emissions significantly higher than the background level were found. These emissions are due to piezonuclear reactions which depend on the different modalities of energy release during the tests. For specimens with sufficiently large size and slenderness, relatively large energy release is expected, and hence a higher probability of neutron emissions at the time of failure. Furthermore, during compression tests under cyclic loading, an equivalent neutron dose was found at the end of the test, by neutron bubble detectors, about two times higher than the ordinary background level. The preliminary results of this study are reported in [4].

Since the analyzed material contains iron, it was supposed and recently proved by microchemical analysis [23], that piezonuclear reactions involving fission of iron into aluminum, or into magnesium and silicon, should have occurred during compression of the specimens. Classically during the process of nuclear fission a neutron strikes a heavy nucleus that splits into two lighter fragments. Each of the two fragments consists of a nucleus with roughly half the neutrons and protons of the original nucleus. This fission process releases a large amount of energy and gamma rays are emitted as well as two or more neutrons that are no longer bound by the fission fragments. These free neutrons are now capable of splitting other heavy nuclei, which then release neutrons that split still more nuclei.

Instead piezonuclear fission reactions consist in new nuclear reactions produced by new methods such as pressure, fracture or cavitation. Even small deviations from classical assumptions, e.g., from the concept of average bond energy per nucleon, could explain these new phenomena. It would suffice to assume a weak section within the nucleus, as it happens in very hard and strong rocks, that nevertheless cleave under very low stresses. The proposed fission of iron into aluminum is supported by very accurate spectroscopical analysis of the fracture surfaces and consistent geological data [23, 24].

The present natural abundances of aluminum (~8 %), and silicon (28 %) and scarcity of iron (~4 %) in the con-

tinental Earth's crust are possibly due to the piezonuclear fission reactions considered above [1–4].

This reaction would be activated where the environment conditions (pressure and temperature) are particularly severe, and mechanical phenomena of fracture, crushing, fragmentation, comminution, erosion, friction, etc., may occur. If we consider the evolution of the percentages of the most abundant elements in the Earth crust during the last 4.5 billion years, we realize that iron and nickel have drastically diminished, whereas aluminum, silicon and magnesium have as much increased. It is also interesting to realize that such increases have developed mainly in the tectonic regions, where frictional phenomena between the continental plates occurred [1–4, 25–27].

## 2. Neutron emission detection techniques

For an accurate neutron evaluation, a  $^3\text{He}$  proportional counter was used. This type of neutron detector must rely upon a conversion process where an incident neutron interacts with a nucleus to produce a secondary charged particle. These charged particles are then detected, and from them the neutrons presence is deduced.

Due to the difficulties in neutron measurements with the presence of an electromagnetic field, electromagnetic emissions were also monitored during compression tests by using a measuring device with working frequency range from Hz up to several MHz. The experimental results [28] show that the typical electromagnetic emissions detected during the tests are included in the frequency range from 160 kHz to 4 MHz. The neutron detectors used are designed and manufactured under a quality system, in compliance with the standard requirements provided by the International Electrotechnical Commission for electromagnetic interference. In particular, the instruments used are insensitive to electromagnetic noise in the frequency range from 150 kHz to 230 MHz, so that no spurious counts were observed during the tests.

### 2.1. $^3\text{He}$ neutron proportional counter

The  $^3\text{He}$  detector used in compression test under displacement control is a  $^3\text{He}$  type (Xeram, France) with electronics of preamplification, amplification and discrimination directly connected to the detector tube. The detector is powered with 1.3 kV, supplied via a high voltage nuclear instrument module (NIM). The output producing the logic pulses is connected to a NIM counter. The logic output of the detector is enabled for analog signals exceeding 300 mV. This discrimination threshold is a consequence of the sensitivity of the  $^3\text{He}$  detector to the gamma rays ensuing neutron emission in ordinary nuclear processes. This value was determined by measuring the analog signal of the detector by means of a Co-60 gamma source. This detector was also calibrated for the measurement of thermal neutrons; its sen-

Table 1

Characteristics of displacement-controlled compression tests on Green Luserna Granite specimens

Granite specimen	Geometry of the specimen			Displacement velocity, mm/s	Peak load, kN	Peak stress, MPa	Time at the peak load, s
	$D$ , mm	$H$ , mm	$\lambda = H/D$				
P1	28	14	0.5	0.001	52.19	84.8	735.0
P2	28	28	1	0.001	33.46	54.4	1239.0
P3	28	56	2	0.001	41.28	67.1	1089.0
P4	53	25	0.5	0.001	129.00	58.5	960.0
P5	53	50	1	0.001	139.10	63.0	2460.0
P6	53	101	2	0.001	206.50	93.6	1180.0
P7	112	60	0.5	0.01	1099.30	111.6	231.3
P8	112	112	1	0.01	1077.10	109.4	263.5
P9	112	224	2	0.01	897.80	91.2	218.6

sitivity is  $65 \text{ cps}/n_{\text{th}}$ . During the experimental measurements, the front-end electronics has been screened with aluminum foils for electromagnetic noise. In addition, the associated measurement system was shielded with polystyrene, in order to avoid possible accidental impact.

## 2.2. Neutron bubble detectors

A set of passive neutron detectors insensitive to electromagnetic noise and with zero gamma sensitivity was used in compression tests under cyclic loading. The dosimeters, based on superheated bubble detectors (BTI, Ontario, Canada) [29], are calibrated at the factory against an AmBe source in terms of NCRP38 [30]. Bubble detectors provide instant visible detection and measurement of neutron dose. Each detector is composed of a polycarbonate vial filled with elastic tissue-equivalent polymer, in which droplets of a superheated gas (freon) are dispersed. When a neutron strikes a droplet, the latter immediately vaporizes, forming a visible gas bubble trapped in the gel. The number of droplets provides a direct measurement of the equivalent neutron dose. These detectors are suitable for neutron integral dose measurements, in the energy ranges of thermal neutrons ( $E = 0.025 \text{ eV}$ ) and fast neutrons ( $E > 100 \text{ keV}$ ).

## 3. Compression tests under monotonic displacement control

### 3.1. Preliminary tests on prismatic specimens

Preliminary tests on prismatic specimens were presented in previous contributions, recently published [1–3], and related to piezonuclear reactions occurring in solids containing iron — samples of granite rocks — in compression. The materials selected for the compression tests were Carrara Marble (calcite) and Green Luserna Granite (gneiss). This choice was prompted by the consideration that, test specimen dimensions being the same, different brittleness numbers [31] would cause catastrophic failure in granite, not in marble. The test specimens were subjected to uniaxial compression to assess scale effects on brittleness [32].

Four test specimens were used, two made of Carrara Marble and two made of Luserna Granite. All of them were of the same size and shape, measuring  $6 \times 6 \times 10 \text{ cm}^3$ . The same testing machine was used on all the test specimens: a standard servo-hydraulic press with a maximum capacity of 500 kN equipped with control electronics. This machine makes it possible to carry out tests in either load control or displacement control. The tests were performed in piston travel displacement control by setting, for all the test specimens, a velocity of 0.001 mm/s during compression. Neutron emission measurements were made by means of a  $^3\text{He}$  detector placed at a distance of 10 cm from the test specimen and enclosed in a polystyrene case, to prevent the results from being altered by impacts or vibrations.

The measurements of neutron emissions obtained on marble yielded values comparable with the background, even at the time of test specimen failure. The neutron measurements obtained on the two granite test specimens, instead, exceeded the background value by about one order of magnitude when catastrophic failure occurred. The first granite test specimen reached at time  $T = 32 \text{ min}$  a peak load of ca 400 kN, corresponding to an average pressure on the bases of 111.1 MPa. When failure occurred, the count rate was found to be:  $(28.3 \pm 0.2) \cdot 10^{-2} \text{ cps}$  corresponding to an equi-

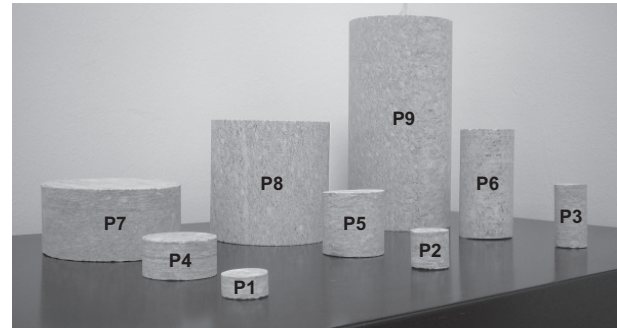


Fig. 1. Green Luserna Granite cylindrical specimens by varying slenderness and size-scale

valent flux of thermal neutrons of  $(43.6 \pm 0.3) \cdot 10^{-4} \times n_{th} \text{ cm}^{-2} \cdot \text{s}^{-1}$ . The second granite test specimen reached at time  $T = 29$  min a peak load of ca 340 kN, corresponding to an average pressure on the bases of 94.4 MPa. When failure occurred, the count rate was found to be:  $(27.2 \pm 0.2) \cdot 10^{-2}$  cps corresponding to an equivalent flux of thermal neutrons of  $(41.9 \pm 0.3) \cdot 10^{-4} n_{th} \text{ cm}^{-2} \cdot \text{s}^{-1}$ .

These phenomena could be caused by piezonuclear reactions that occurred in the granite but did not in the marble. Moreover, granite contains iron, which appears to be the most favourable element for the production of piezonuclear reactions [1–3]. These experimental evidences induced the authors to carry out further tests on cylindrical Green Luserna Granite specimens of different size and shape.

### 3.2. Tests on cylindrical specimens

#### 3.2.1. Experimental set-up

Neutron emissions were measured on nine Green Luserna Granite cylindrical specimens, of different size and shape (Table 1, Fig. 1), denoted with P1, P2, ..., P9 [4]. The compression tests were carried out by means of a servo-hydraulic press, with a maximum capacity of 1800 kN, working by a digital type electronic control unit. The management software was TESTXPRTII by Zwick/Roel (Zwick/Roel Group, Ulm, Germany), while the mechanical parts are manufactured by Baldwin (Instron Industrial Products Group, Grove City, PA, USA). The force applied was determined by measuring the pressure in the loading cylinder by means of a transducer. The margin of error in the determination of the force is 1 %, which makes it a class 1 mechanical press. The specimens were arranged with the two smaller surfaces in contact with the press platens, without coupling materials in-between, according to the testing modalities known as “test by means of rigid platens with friction”. The platen was controlled by means of a wire-type potentiometric displacement transducer. The tests were performed under displacement control with the planned displacement velocities ranging from 0.001 to 0.01 mm/s.

Due to natural radionuclide presence in Green Luserna Granite an estimation of ambient gamma radiation dose rate was performed on the nine specimens before the compression tests in order to make sure that the natural specimen radiation level does not provide “spurious” counts in neutron measurement. A gamma radiation monitor device (AT6130, ATOMTEX) was used. The data acquisition time was fixed at 600 s, and the specimen radiation level was measured. Typical gamma radiation level for this type of granite was found and compared with the natural gamma background in room condition. The experimental results are reported in Table 2.

For Green Luserna Granite the gamma radiation component is mainly due to the natural radionuclide in granite composition: Ra-226 (ca. 125 Bq/Kg, decay gamma rays energy 186.1 keV), Th-232 (ca. 114 Bq/Kg, decay gamma

Table 2  
Ambient gamma radiation dose rate measurements

Specimen	Ambient gamma radiation dose rate, $\mu\text{Sv/h}$
Background	$0.07 \pm 14 \%$
P1	$0.10 \pm 16 \%$
P2	$0.11 \pm 17 \%$
P3	$0.09 \pm 17 \%$
P4	$0.11 \pm 15 \%$
P5	$0.09 \pm 11 \%$
P6	$0.09 \pm 11 \%$
P7	$0.15 \pm 14 \%$
P8	$0.12 \pm 10 \%$
P9	$0.13 \pm 11 \%$

rays energy 63.81 keV and 140.88 keV), and K-40 (ca. 1276 Bq/Kg, decay gamma rays energy 1460.83 keV). Considering the type and the intensity of natural radionuclide activity in granite and thanks to the logic output discrimination threshold fixed on the  $^3\text{He}$  proportional counter (300 mV), no “spurious” signal was detected.

The  $^3\text{He}$  neutron detector was switched on at least one hour before the beginning of each compression test, in order to reach the thermal equilibrium of electronics, and to make sure that the behaviour of the devices was stable with respect to intrinsic thermal effects. The detector was placed in front of the test specimen at a distance of 20 cm and it was enclosed in a polystyrene case of 10 cm of thickness in order to avoid “spurious” signals coming from impacts and vibrations.

A relative measurement of natural neutron background was performed in order to assess the average background affecting data acquisition in experimental room condition. The  $^3\text{He}$  device was positioned in the same condition of the experimental set-up and the background measures were performed fixing at 60 s the acquisition time, during a

Table 3  
Neutron emission experimental data on Green Luserna Granite specimens

Granite specimen	Average neutron background, $10^{-2}$ cps	Count rate at the neutron emission, $10^{-2}$ cps
P1	$3.17 \pm 0.32$	$8.33 \pm 3.73$
P2	$3.17 \pm 0.32$	Background
P3	$3.17 \pm 0.32$	Background
P4	$3.83 \pm 0.37$	Background
P5	$3.84 \pm 0.37$	$11.67 \pm 4.08$
P6	$4.74 \pm 0.46$	$25.00 \pm 6.01$
P7	$4.20 \pm 0.80$	Background
P8	$4.20 \pm 0.80$	$30.00 \pm 11.10$
P9	$4.20 \pm 0.80$	$30.00 \pm 10.00$



preliminary period of more than three hours, for a total number of 200 counts. The average measured background level is ranging from  $(3.17 \pm 0.32) \cdot 10^{-2}$  to  $(4.74 \pm 0.46) \cdot 10^{-2}$  cps (see Table 3).

### 3.2.2. Experimental results

Additional background measurements were repeated before each test, fixing an acquisition time of 60 s, up to the assessment of no significant variation in natural background. Neutron measurements of specimens P2, P3, P4, P7 yielded values comparable with the ordinary natural background, whereas in specimens P1 and P5 the experimental data exceeded the background value by about four times. Instead, for specimens P6, P8 and P9, the neutron emissions achieved values one order of magnitude higher than ordinary background. In Fig. 2 the load vs. time diagram and the neutron count rate evolution for specimens P6, P8 and P9 are shown. In Table 3, experimental data concerning compression tests on the nine Green Luserna Granite specimens are summarized.

The preliminary experimental results described above and reported in [1–3] are confirmed by those obtained from compression tests on the cylindrical specimens. Neutron emissions related to specimens with very brittle or catastrophic failure result to be larger by about one order of magnitude than the ordinary background (see Fig. 2).

The maximum neutron emissions were obtained from test specimens characterized with a volume large than a threshold value of about  $360 \text{ cm}^3$ .

In addition, the experimental results seem to demonstrate that neutron emissions follow an anisotropic and impulsive distribution from a specific zone of the specimen. It is a matter of fact that the detected neutron flux and consequently neutron dose are inversely proportional to the square of the distance from the source. For these reasons, the  $^3\text{He}$  device could have underestimated neutron flux intensity. A possible solution to avoid underestimated data acquisition is an experimental measurement by using more than one  $^3\text{He}$  detector and more bubble dosimeters placed around the test specimens.

## 4. Compression tests under cyclic loading

### 4.1. Experimental set-up

Neutron emissions from compression test under cyclic loading were also detected by using neutron bubble detectors. Due to their isotropic angular response, three bubble detectors for thermal neutrons and three bubble detectors for fast neutrons were positioned at a distance of about 5 cm, all around the specimen. The detectors had been previously activated, unscrewing the protection cap, in order to reach the suitable thermal equilibrium, and they were kept active for all the test duration. Furthermore, a thermal neutron bubble detector and a fast neutron bubble detector were used for the background control during the test. Three dif-

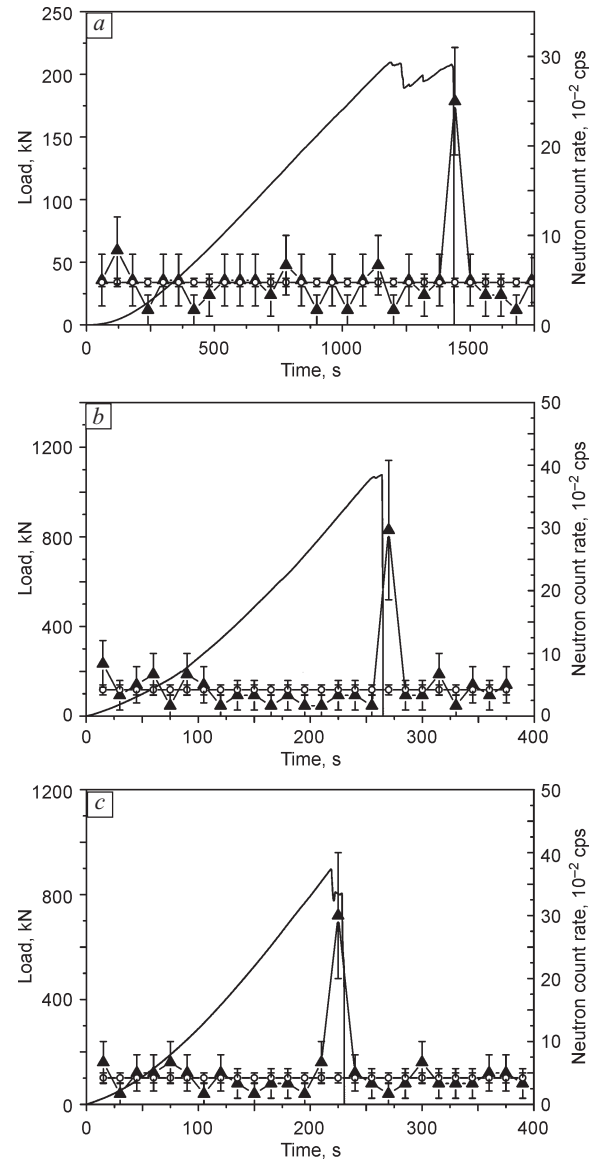


Fig. 2. Specimens P6 (a), P8 (b), P9 (c). Load vs. time diagrams (—) and neutron count rate for Green Luserna Granite:  $D = 53$  (a), 112 mm (b, c) and  $H = 101$  (a), 112 (b), 224 mm (c) ( $\blacktriangle$ ;  $\diamond$  — average neutron background:  $(4.74 \pm 0.46) \cdot 10^{-2}$  (a) and  $(4.20 \pm 0.80) \cdot 10^{-2}$  cps (b, c)

ferent tests were performed on Green Luserna Granite specimens with the same shape and size ( $D = 53 \text{ mm}$ ,  $H = 53 \text{ mm}$ ,  $\lambda = 1$ ).

The cyclic loading was fixed at a frequency of 2 Hz for the three specimens. The load excursion was programmed respectively from a minimum load of 15 kN to a maximum of 110 kN during the first cyclic loading trial, from a minimum load of 12 kN to a maximum of 85 kN in the second test, and from a minimum of 10 kN to a maximum of 60 kN during the third test. Test durations were approximately of 1126 min, 21 min, and 5026 min, respectively. The experimental results are summarized in Table 4.

Table 4

Compression test under cyclic loading. Neutron emission experimental data on Green Luserna Granite specimens

Test	Min–max load, kN	Test duration, min	Average neutron background, nSv/h	Equivalent neutron dose at the end of the test, nSv/h	Equivalent neutron dose to neutron background ratio
1	15–110	1 126	$26.32 \pm 5.26$	$45.77 \pm 9.15$	$1.74 \pm 0.35$
2	12–85	21	$27.77 \pm 5.56$	$59.29 \pm 11.86$	$2.14 \pm 0.43$
3	10–60	5 026	$13.98 \pm 2.76$	$28.74 \pm 5.75$	$2.06 \pm 0.41$

#### 4.2. Experimental results

Droplet counting was performed every 12 hours and the equivalent neutron dose was calculated. In the same way, the natural background was estimated by means of the two bubble dosimeters used for assessment.

In the first test the background was found to be  $(26.32 \pm 5.26)$  nSv/h. A significant increment in the neutron emission with respect to the background level was detected at specimen failure. The equivalent neutron dose at the end of the test was  $(45.77 \pm 9.15)$  nSv/h.

The background associated to the second test was of  $(27.77 \pm 5.56)$  nSv/h. The neutron dose variation was found to be more than twice higher with respect to ordinary

background,  $(59.29 \pm 11.86)$  nSv/h. In this test, bubbles were formed concurrently to specimen failure. In spite of the very short duration of the test, droplets reading was performed after 12 hours, and compared with the natural background value. In this way it was possible to reduce experimental uncertainty related to equivalent neutron dose evaluation.

Finally, during the third trial the ordinary background was found to be  $(13.98 \pm 2.76)$  nSv/h. The neutron equivalent dose variation, evaluated during the third cyclic loading test, is reported in Fig. 3 [4]. Also in this case, an increment of more than twice with respect to the background level was detected at specimen failure. No significant variations in neutron emissions were observed before the failure. The equivalent neutron dose at the end of the test was  $(28.74 \pm 5.75)$  nSv/h (Table 4).

The comparison between background equivalent neutron dose and equivalent neutron dose at the end of the cyclic loading tests are reported in Fig. 4. From Table 3, considering the sensitivity of bubble detectors (20 %), it is possible to observe that in each test the average increment in equivalent neutron dose at failure is about twice higher than the natural neutron background.

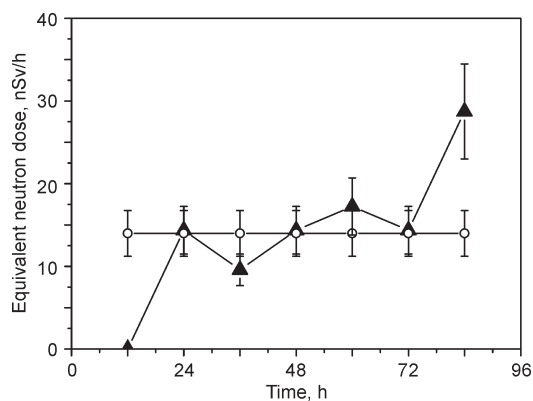


Fig. 3. Compression test under cyclic loading. Equivalent neutron dose ( $\blacktriangle$ ) variation during the third test on Green Luserna Granite specimen;  $\circ$  — average neutron background ( $13.98 \pm 2.76$ ) nSv/h

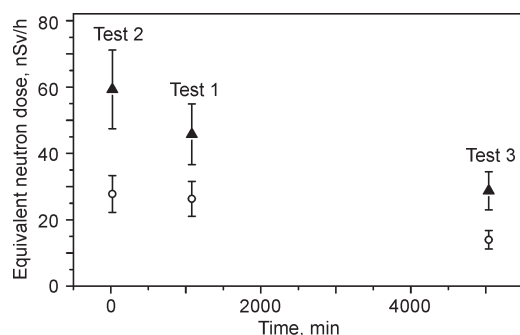


Fig. 4. Compression tests under cyclic loading. Comparison between the background equivalent neutron dose ( $\circ$ ) and the equivalent neutron dose at the end of the tests ( $\blacktriangle$ )

#### 5. Conclusions

Neutron emission measurements were performed on Green Luserna Granite specimens during mechanical tests. From these experiments, it can be clearly seen that piezonuclear reactions giving rise to neutron emissions are possible in inert non-radioactive solids under loading. In particular, during compression tests of specimens with sufficiently large size, the neutron flux was found to be of about one order of magnitude higher than the background level at the time of catastrophic failure. For test specimens with more ductile behaviour, neutron emissions significantly higher than the background were also found. Neutron detection is also confirmed in compression tests under cyclic loading.

#### Acknowledgements

The financial support provided by the Regione Piemonte (Italy) RE-FRESCOS Project is gratefully acknowledged.

#### References

- [1] A. Carpinteri, F. Cardone and G. Lacidogna, Piezonuclear neutrons from brittle fracture: Early results of mechanical compression tests, *Strain*, 45 (2009) 332.

- [2] F. Cardone, A. Carpinteri and G. Lacidogna, Piezonuclear neutrons from fracturing of inert solids, *Phys. Lett. A*, 373, No. 45 (2009) 4158.
- [3] A. Carpinteri, F. Cardone and G. Lacidogna, Energy emissions from failure phenomena: Mechanical, electromagnetic, nuclear, *Exp. Mech.*, 50, No. 8 (2009) 1235.
- [4] A. Carpinteri, G. Lacidogna, A. Manuello and O. Borla, Evidence of Piezonuclear Reactions: From Geological and Tectonic Transformations to Neutron Detection and Measurements, in *Proc. SEM Annual Conference & Exposition on Experimental and Applied Mechanics, Indianapolis, 7–10 June 2010*, Paper No. 458 (2010).
- [5] K. Mogi, Study of elastic shocks caused by the fracture of heterogeneous materials and its relation to earthquake phenomena, *B. Earthq. Res. I. Tokyo*, 40 (1962) 125.
- [6] D.A. Lockner, J.D. Byerlee, V. Kuksenko, A. Ponomarev and A. Sidorin, Quasi-static fault growth and shear fracture energy in granite, *Nature*, 350, No. 6313 (1991) 39.
- [7] M. Ohtsu, The history and development of acoustic emission in concrete engineering, *Mag. Concrete Res.*, 48, No. 177 (1996) 321.
- [8] R. Shcherbakov and D.L. Turcotte, Damage and self-similarity in fracture, *Theor. Appl. Fract. Mech.*, 39, No. 3 (2003) 245.
- [9] A. Carpinteri, G. Lacidogna and N. Pugno, Richter's laws at the laboratory scale interpreted by acoustic emission, *Mag. Concrete Res.*, 58, No. 9 (2006) 619.
- [10] A. Carpinteri, G. Lacidogna and G. Niccolini, Critical behaviour in concrete structures and damage localization by acoustic emission, *Key Eng. Mater.*, 312 (2006) 305.
- [11] A. Carpinteri, G. Lacidogna and N. Pugno, Structural damage diagnosis and life-time assessment by acoustic emission monitoring, *Eng. Fract. Mech.*, 74, No. 1–2 (2007) 273.
- [12] A. Carpinteri, G. Lacidogna and G. Niccolini, Fractal analysis of damage detected in concrete structural elements under loading, *Chaos Soliton. Fract.*, 42, No. 4 (2009) 2047.
- [13] A. Carpinteri, G. Lacidogna and S. Puzzi, From criticality to final collapse: Evolution of the “b-value” from 1.5 to 1.0, *Chaos Soliton. Fract.*, 41, No. 2 (2009) 843.
- [14] A. Carpinteri, G. Lacidogna, G. Niccolini and S. Puzzi, Morphological fractal dimension versus power-law exponent in the scaling of damaged media, *Int. J. Damage Mech.*, 18, No. 3 (2009) 259.
- [15] M. Miroshnichenko and V. Kuksenko, Study of electromagnetic pulses in initiation of cracks in solid dielectrics, *Sov. Phys. Solid State*, 22 (1980) 895.
- [16] J.W. Warwick, C. Stoker and T.R. Meyer, Radio emission associated with rock fracture: Possible application to the Great Chilean earthquake of May 22, 1960 *J. Geophys. Res.*, 87, No. B4 (1982) 2851.
- [17] S.G. O'Keefe and D.V. Thiel, A mechanism for the production of electromagnetic radiation during fracture of brittle materials, *Phys. Earth Planet. Int.*, 89, No. 1–2 (1995) 127.
- [18] D.F. Scott, T.J. Williams and S.J. Knoll, Investigation of Electromagnetic Emissions in a Deep Underground Mine, in *Proc. 23rd Int. Conf. Ground Control in Mining, Morgantown, 3–5 August 2004* (2004) 125.
- [19] V. Frid, A. Rabinovitch and D. Bahat, Fracture induced electromagnetic radiation, *J. Phys. D. Appl. Phys.*, 36, No. 13 (2003) 1620.
- [20] A. Rabinovitch, V. Frid and D. Bahat, Surface oscillations — A possible source of fracture induced electromagnetic radiation, *Tectonophysics*, 431, No. 1–4 (2007) 15.
- [21] G. Lacidogna, A. Carpinteri, A. Manuello, G. Durin, A. Schiavi, G. Niccolini and A. Agosto, Acoustic and electromagnetic emissions as precursor phenomena in failure processes, *Strain* (2010) doi: 10.1111/j.1475-1305.2010.00750.x.
- [22] A. Carpinteri, G. Lacidogna, A. Manuello, A. Niccolini, A. Schiavi and A. Agosto, Mechanical and electromagnetic emissions related to stress-induced cracks, *Exp. Techniques* (2010) (*in print*).
- [23] A. Carpinteri, A. Chiodoni, A. Manuello and R. Sandrone, Compositional and microchemical evidence of piezonuclear fission reactions in rock specimens subjected to compression tests, *Strain* (2010) doi: 10.1111/j.1475-1305.2010.00767.x.
- [24] A. Carpinteri and A. Manuello, Geomechanical and geochemical evidence of piezonuclear fission reactions in the Earth's crust, *Strain* (2010) doi: 10.1111/j.1475-1305.2010.00766.x.
- [25] A.D. Anbar, Elements and evolution, *Science*, 322, No. 5907 (2008) 1481.
- [26] G. Favero and P. Jobstraibizer, The distribution of aluminum in the Earth: From cosmogenesis to Sial evolution, *Coord. Chem. Rev.*, 149 (1996) 467.
- [27] K.O. Konhauser, E. Pecoits, S.V. Lalonde, D. Papineau, E.G. Nisbet, M.E. Barley, N.T. Arndt, K. Zahnle and B.S. Kamber, Oceanic nickel depletion and a methanogen famine before the Great Oxidation Event, *Nature*, 458, No. 7239 (2009) 750.
- [28] G. Lacidogna, A. Manuello, A. Carpinteri, G. Niccolini, A. Agosto and G. Durin, Acoustic and Electromagnetic Emissions in Rocks under Compression, in *Proc. SEM Annual Conference & Exposition on Experimental and Applied Mechanics, Indianapolis, 7–10 June 2010*, Paper No. 433 (2010).
- [29] Bubble Technology Industries, Instruction Manual for the Bubble Detector, Chalk River, Ontario, Canada, 1992.
- [30] National Council on Radiation Protection and Measurements, Protection Against Neutron Radiation, NCRP Report 38, 1971.
- [31] A. Carpinteri, Cusp catastrophe interpretation of fracture instability, *J. Mech. Phys. Solids*, 37, No. 5 (1989) 567.
- [32] A. Carpinteri, A catastrophe theory approach to fracture mechanics, *Int. J. Fract.*, 44, No. 1 (1990) 57.